The Propagation of Ultrasonic Waves through a Bubbly Liquid into Tissue: A Linear Analysis

Quan Qi, William D. O'Brien Jr., *Fellow, IEEE*, and John G. Harris

***Abstract*—The steady-state response induced by a harmonically driven, ultrasonic wave in a structure comprised of two layers, the first a bubbly liquid, and the second a viscoelastic solid with a rigid boundary, is studied in the linear approximation. This structure is intended to model a cavitating liquid in contact with tissue. The upper surface of the liquid is driven harmonically and models the source. The lower surface of the solid is rigid and models the bone. While cavitation is inherently nonlinear, the propagation process is approximated as linear. The transient response is not calculated. The model of the bubbly liquid is a simple continuum one, supplemented by allowing for a distribution of different equilibrium bubble radii and for the relaxation of the oscillations of each bubble. The model contains three functions, the probability distribution describing the distribution of bubble radii, and two functions modeling the mechanical response of the individual bubble and the tissue, respectively. Numerical examples are worked out by adapting data taken from various published sources to deduce the parameters of these functions. These examples permit an assessment of the overall attenuation of the structure, and of the magnitudes of the pressure and particle velocity in the bubbly liquid and of the traction and the particle displacement in the tissue.**

I. Introduction

THE STEADY-state response of a layered structure comprised of a bubbly liquid layer and a viscoelastic solid layer is studied. The structure models a cavitating liquid in contact with tissue. It is of interest because ultrasonic devices designed to clean the surface of tissue are being used (HYDROSOUND^{TM}, Arjo, Inc., Morton Grove, IL) and accordingly there is considerable interest in what happens at the interface. Our current understanding of ultrasonic cleaning is that collapsing bubbles with their concurrent jet formation [3] at a surface are largely responsible for cleaning. However, though our motivation is an interest in cleaning, our goal here is not to study the cleaning, but rather to study the propagation processes, using a viscoelastic model for the tissue and a simple model for the cavitating liquid. This will help us to understand the average mechanical response of the overall structure and form a first step towards modeling the role played by the tissue. Moreover, though this structure has a rich transient response we confine our study to the steady-state response, in part because it is the most relevant to the application of interest and in part because our model does not adequately take account of the initiation of the cavitation.

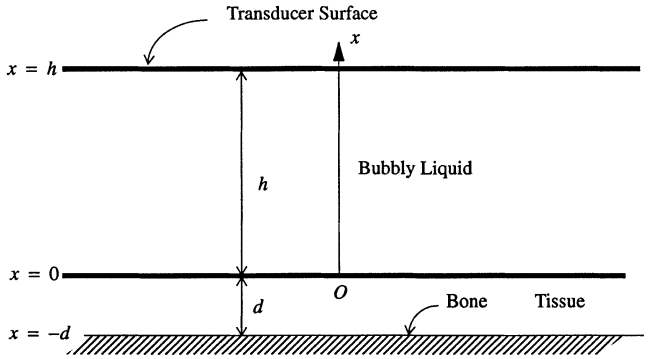

Fig. 1. The geometry of the problem. The origin is at the tissue surface.

Wijngaarden [10], [11] developed a simple continuum model of the mechanical response of a liquid filled with bubbles (a bubbly liquid) in which the bubbles, which behave as oscillators, rather than the liquid itself, provide the compressibility. With this model he calculated the dispersion and attenuation caused by the bubbles. Using a more complete linear model, that contains the effects of liquid compressibility and bubble-size distribution, Commander and Prosperetti [1] also studied linear propagation in a bubbly liquid finding satisfactory agreement between their theory and experiments done by others. An approximate attempt to study a driven acoustic wavefield in a bubbly liquid confined by a transducer and a rigid plane was made by Hanson *et al.* [4]. We use a linearization of Wijngaarden's theory to model the liquid layer supplemented by a relation taken from [1] that permits the bubble radii to vary, and by a heuristic relation that takes approximate account of the bubbles' relaxation mechanisms. We model the tissue layer using a linear viscoelastic model suggested in [2], though we modify it slightly to make it regular for large time.

II. Formulation

In Fig. 1 we show the tissue surface at $x = 0$, a driving transducer at $x = h$ and the bone at $x = -d$. The bubbly liquid is confined between the deformable tissue surface and the transducer, while between the tissue surface and the bone lie the epidermis, dermis and subcutaneous fat. The driving

Manuscript received September 20, 1993; revised March 21, 1994 and August 22, 1994; accepted August 22, 1994. This work was supported by the Manufacturing Research Center at UIUC, National Science Foundation Grant No. MSS-9114547, and Arjo, Inc.

Q. Qi and J. G. Harris are with the Department of Theoretical and Applied Mechanics, University of Illinois, Urbana, IL 61801 USA.

W. D. O'Brien Jr. is with the Department of Electrical and Computer Engineering, University of Illinois, Urbana, IL 61801 USA.

IEEE Log Number 9406689.

frequency of the transducer is of the order of 30 kHz. We assume that the bubble radius R_0 is of the order of 0.5 μm to 5 μm. We shall work with linear approximations to the equations of motion written in terms of dimensionless variables. The amplitude of the excitation velocity at the transducers surface is $\epsilon\nu_0$, where $\epsilon < 1$ is a small parameter. The dimensionless space and time variables are $x_1 = x/h$ and $t_1 = \omega_0 t$, where x is the spatial coordinate, t is the time and ω_0 is the driving frequency of the source. The remaining symbols will be defined as they appear. A subscript 1 is used to denote dimensionless quantities.

The following are the equations for the bubbly liquid between $1 \geq x_1 \geq 0$.

$$\frac{\partial \rho_1}{\partial t_1} + \frac{\nu_0}{\omega_0 h}\frac{\partial \nu_1}{\partial x_1} = 0, \tag{1}$$

$$\frac{\partial \nu_1}{\partial t_1} + \frac{p_0}{\rho_0(1-\beta_0)\nu_0\omega_0 h}\frac{\partial p_1}{\partial x_1} = 0, \tag{2}$$

and

$$\rho_1 = -\frac{4\pi}{1-\beta_0}\int_0^\infty R_0^3 R_1(R_0;t_1,x_1)\, f(R_0,x_1)\, dR_0. \tag{3}$$

Equation (1) is the linearized mass conservation, (2) is the momentum conservation, and (3), suggested in [1], is obtained from a relation between average density and volume fraction of the bubbles. The terms ρ_1, ν_1 and p_1 are the dimensionless perturbations in density, particle velocity and pressure. The corresponding dimensional quantities are given by $\rho = \rho_0(1-\beta_0)(1+\epsilon\rho_1), \nu = \epsilon\nu_0\nu_1$ and $p = p_0(1+\epsilon p_1)$. The terms ρ_0 and p_0 are the equilibrium density and pressure. The function $f(R_0, x_1)$ is a distribution function for the bubble radii whose unperturbed radii are R_0. The term R_1 is the dimensionless perturbation to the bubble radius and the corresponding dimensional bubble radius $R = R_0(1+\epsilon R_1)$. The number of bubbles per unit volume with equilibrium radius between R_0 and $R_0 + dR_0$ is given by $dN = f(R_0, x_1)\, dR_0$ and the equilibrium volume fraction β_0 is given by

$$\beta_0 = \frac{4\pi}{3}\int_0^\infty R_0^3 f(R_0;x_1)\, dR_0. \tag{4}$$

In general R_1 depends on the corresponding equilibrium radius R_0, as well as on x_1 and t_1.

For the tissue between $0 > x_1 > -d/h$ the governing equations are

$$\frac{\partial^2 u_1}{\partial t_1^2} = \frac{p_0}{\rho_s h \nu_0 \omega_0}\frac{\partial \sigma_1}{\partial x_1}, \tag{5}$$

$$\frac{\partial u_1}{\partial x_1} = \frac{\omega_0 p_0 h J_T(0)}{\nu_0}\left[\int_{0-}^{t_1} J_{T1}(t_1-\tau)\frac{\partial \sigma_1}{\partial \tau}d\tau\right]. \tag{6}$$

The terms u_1 and σ_1 are the dimensionless perturbations in particle displacement and normal traction. Their dimensional counterparts are given by $u = \epsilon\omega_0^{-1}\nu_0 u_1$ and $\sigma = p_0\epsilon\sigma_1$. The term ρ_s is the average unperturbed tissue density. The function $J_{T1}(t_1) = J_T(0)J_{T1}(t_1)$ is the dimensional creep compliance and $J_T(0)$ is its initial value. Equation (5) is the momentum conservation and (6) is the constitutive relation for the tissue. The dimensionless function J_{T1} is explained in the discussion section.

We have written (6) in the time domain rather than in the frequency domain because the function J_{T1} was arrived at by fitting a creep function to data measured quasi-statically over a time period in which the tissue flows somewhat as a liquid. Eventually, the deformation of the tissue will have become so large as to violate the assumption of linearity. To Fourier transform J_{T1} we must modify its long time behavior in such a way that its short time behavior is largely unaltered. Further, the irreversible nature of the function means that it has an initial condition built into it making it easier to assume that the structure is quiescent until $t = 0^-$, and subsequently to extract the steady-state behavior.

It remains to complete the model for the bubbly liquid. By analogy with the model for the tissue we include relaxation in the linearized Rayleigh-Plesset equation as follows.

$$\frac{\partial^2 R_1}{\partial t_1^2} + \Omega^2 R_1 = -\frac{p_0}{\rho_0 R_0^2\omega_0^2}p_1 + \frac{J_B(0)}{\rho_0 R_0^2\omega_0^2} \cdot \int_0^{t_1} J_{B1}(t_1-\tau)\frac{\partial R_1}{\partial \tau}d\tau \tag{7}$$

The function $J_B(t_1) = J_B(0)\, J_{B1}(t_1)$ describes the viscoelastic behavior of the bubble oscillations and $J_B(0)$ is its initial value. It enters the linearized Rayleigh-Plesset equation in a way analogous to that in which the creep compliance enters the equations describing the tissue. We shall approximate J_{B1} in the frequency domain in ways that emulate relaxation mechanisms determined from experiments or more accurate models. Note that by taking J_{B1} to be a delta function the usual viscous damping is recovered. The dimensionless natural frequency Ω is given by

$$\Omega^2 = \frac{1}{\rho_0(R_0\omega_0)^2}\left[3p_{g0} - \frac{2\Gamma}{R_0}\right], \tag{8}$$

where Γ denotes the surface tension coefficient and p_{g0} is the equilibrium pressure in the bubble.

We have written (7) in the time domain for three interrelated reasons. Firstly, by including a convolution integral of this form it is possible to recover the linear model in [1, pp. 31–33] in the frequency domain, provided the result is simplified to account for our assumption of incompressibility. Secondly, as already stated, it exhibits the global similarities between the two materials, despite their numerous differences in detail. Lastly, by writing (7) in the time domain, it is clear that the compressibility of the bubbly liquid is provided by the bubbles behaving as oscillators whose response is not entirely elastic. This is not immediately apparent from the frequency domain result to be given by (16). Note, however that this model does not take account of the formation of the bubbles. They are instantaneously present. Moreover, it only implicitly includes the thermal effects through the function J_{B1}.

Finally, the corresponding dimensionless boundary and continuity conditions are

$$\nu_1 = H(t_1)\,\mathrm{Re}(e^{it_1}), \qquad x_1 = 1, \tag{9}$$

$$\nu_1 = \frac{\partial u_1}{\partial t_1}, \qquad \sigma_1 = -p_1, \qquad x_1 = 0, \tag{10}$$

where $H(t_1)$ is the Heaviside function, and

$$u_1 = 0, \qquad x = -\frac{d}{h}. \tag{11}$$

III. Solutions

To map to the frequency domain we use the following Fourier transform pair.

$$\overline{f}(\omega) = \frac{1}{(2\pi)^{1/2}} \int_{-\infty}^{\infty} f(t_1) e^{-i\omega t_1}\, dt_1,$$
$$f(t_1) = \frac{1}{(2\pi)^{1/2}} \int_{-\infty}^{\infty} \overline{f}(\omega) e^{i\omega t_1}\, d\omega. \tag{12}$$

Note that for $f(t_1)$ to be 0 for $t_1 < 0, \overline{f}(\omega)$ must be analytic throughout the $\mathrm{Im}(\omega) < 0$ half plane. Further note that for $f(t_1)$ to be real $\overline{f}(\omega) = \overline{f}^c(-\omega)$, where the superscript c indicates complex conjugate. These observations are used when taking the transform of $J_{T1}(t_1)$ and when indicating how to analytically continue $\overline{J}_{B1}(\omega)$ so that $J_{B1}(t_1)$ can be recovered.

The transformed terms are given by the previously defined symbols but have an overbar. The argument ω may also be indicated. Equations (1)–(3) and (7) become

$$\frac{d}{dx_1}\overline{\nu}_1(\omega, x_1) = -i\omega \frac{h\omega_0}{\nu_0} \overline{p}_1(\omega, x_1), \tag{13}$$
$$\frac{d}{dx_1}\overline{p}_1(\omega, x_1) = -i\omega \frac{\rho_0(1-\beta_0)\nu_0\omega_0 h}{p_0} \overline{\nu}_1(\omega, x_1), \tag{14}$$
$$\overline{p}_1(\omega, x_1) = -\frac{4\pi}{1-\beta_0} \int_0^{\infty} R_0^3 \overline{R}_1(R_0; \omega, x_1) \cdot f(R_0, x_1)\, dR_0, \tag{15}$$

and

$$\overline{p}_1(\omega, x_1) = \frac{\rho_0 R_0^2 \omega_0^2}{p_0} \left[\omega^2 - \Omega^2 + \frac{i\omega(2\pi)^{1/2} J_B(0) \overline{J}_{B1}(\omega)}{\rho_0 R_0^2 \omega_0^2}\right] \cdot \overline{R}_1(R_0; \omega, x_1). \tag{16}$$

Moreover, (5) and (6) become

$$\frac{d}{dx_1}\overline{\sigma}_1(\omega, x_1) = -\frac{\rho_s h \nu_0 \omega_0}{p_0} \omega^2 \overline{u}_1(\omega, x_1) \tag{17}$$

and

$$\frac{d}{dx_1}\overline{u}_1(\omega, x_1) = \frac{(2\pi)^{1/2} p_0 h J_T(0) \omega_0}{\nu_0} \cdot \overline{\sigma}_1(\omega, x_1) i\omega \overline{J}_{T1}(\omega). \tag{18}$$

Finally, the transformed boundary and continuity conditions, (9)–(11), become

$$\overline{\nu}_1(\omega, 1) = \frac{1}{i(\omega - 1)\sqrt{2\pi}}, \tag{19}$$
$$\overline{\nu}_1(\omega, 0) = i\omega \overline{u}_1(\omega, 0), \overline{\sigma}_1(\omega, 0) = -\overline{p}_1(\omega, 0) \tag{20}$$

and

$$\overline{u}_1(\omega, -d/h) = 0. \tag{21}$$

Note that the contour for the inverse transform would pass below the pole at $\omega = 1$.

Equations (13)–(16) may be combined to give

$$\frac{d}{dx_1}\begin{bmatrix}\overline{p}_1 \\ \overline{\nu}_1\end{bmatrix} + i\omega \begin{bmatrix}0 & a_1 \\ a_2 & 0\end{bmatrix}\begin{bmatrix}\overline{p}_1 \\ \overline{\nu}_1\end{bmatrix} = 0, \tag{22}$$

where

$$a_1 = \frac{\rho_0 \nu_0 \omega_0 h(1-\beta_0)}{p_0}, \tag{23}$$
$$a_2 = \left(\frac{4\pi}{1-\beta_0}\right)\frac{p_0\omega_0 h}{\rho_0\nu_0} \cdot \int_0^{\infty} \frac{R_0^3 f(R_0, x_1)\, dR_0}{[3\beta_0 c_0^2 - \omega^2\omega_0^2 R_0^2 - i\omega(2\pi)^{1/2} J_B(0)\overline{J}_{B1}/\rho_0]} \tag{24}$$

and

$$c_0^2 = \frac{p_{g0}}{\rho_0\beta_0} - \frac{2\Gamma}{3\beta_0\rho_0 R_0} = \frac{(R_0\omega_0)^2}{3\beta_0}\Omega^2. \tag{25}$$

The term c_0 is the sound speed in a bubbly liquid having a uniform equilibrium bubble radius R_0 [5]. The solution to (22) is

$$\begin{bmatrix}\overline{p}_1 \\ \overline{\nu}_1\end{bmatrix} = \begin{bmatrix}-\sqrt{a_1/a_2}(iA_0 \sin \overline{\lambda}x_1 + B_0 \cos \overline{\lambda}x_1) \\ A_0 \cos \overline{\lambda}x_1 + iB_0 \sin \overline{\lambda}x_1\end{bmatrix} \tag{26}$$

where $\overline{\lambda} = \sqrt{a_1 a_2}\omega$, and A_0 and B_0 are constants of integration. Similarly, (17) and (18) may be combined to give

$$\frac{d}{dx_1}\begin{bmatrix}\overline{\sigma}_1 \\ i\omega\overline{u}_1\end{bmatrix} + i\omega \begin{bmatrix}0 & b_1 \\ b_2 & 0\end{bmatrix}\begin{bmatrix}\overline{\sigma}_1 \\ i\omega\overline{u}_1\end{bmatrix} = 0, \tag{27}$$

where

$$b_1 = -p_s \frac{h\nu_0\omega_0}{p_0} \tag{28}$$

and

$$b_2 = -\frac{(2\pi)^{1/2} h\omega_0 p_0 J_T(0)}{\nu_0} i\omega \overline{J}_{T1}(\omega). \tag{29}$$

As with (22) the solution to (27) is

$$\begin{bmatrix}\overline{\sigma}_1 \\ \overline{u}_1\end{bmatrix} = \begin{bmatrix}-\sqrt{b_1/b_2}(iC_0 \sin \hat{\lambda}x_1 + D_0 \cos \hat{\lambda}x_1) \\ C_0 \cos \hat{\lambda}x_1 + iD_0 \sin \hat{\lambda}x_1\end{bmatrix}, \tag{30}$$

where $\hat{\lambda} = \sqrt{b_1 b_2}\omega$, and C_0 and D_0 are constants of integration.

Applying the boundary and continuity conditions, we find,

$$\overline{p}_1 = -\sqrt{\frac{a_1}{a_2}} \frac{\sin \hat{\lambda}\frac{d}{h} \sin \overline{\lambda}x_1 + \sqrt{\frac{a_2 b_1}{a_1 b_2}} \cos \hat{\lambda}\frac{d}{h} \cos \overline{\lambda}x_1}{\sin \hat{\lambda}\frac{d}{h} \cos \overline{\lambda} - \sqrt{\frac{a_2 b_1}{a_1 b_2}} \cos \hat{\lambda}\frac{d}{h} \sin \overline{\lambda}} \cdot \frac{1}{(\omega - 1)\sqrt{2\pi}}, \tag{31}$$

$$\overline{v}_1 = \frac{\sin\hat{\lambda}\frac{d}{h}\cos\overline{\lambda}x_1 - \sqrt{\frac{a_2b_1}{a_1b_2}}\cos\hat{\lambda}\frac{d}{h}\sin\overline{\lambda}x_1}{\sin\hat{\lambda}\frac{d}{h}\cos\overline{\lambda} - \sqrt{\frac{a_2b_1}{a_1b_2}}\cos\hat{\lambda}\frac{d}{h}\sin\overline{\lambda}} \cdot \frac{1}{(\omega-1)i\sqrt{2\pi}}, \tag{32}$$

$$\overline{\sigma}_1 = \sqrt{\frac{b_1}{b_2}}\frac{\cos\hat{\lambda}\left(x_1+\frac{d}{h}\right)}{\sin\hat{\lambda}\frac{d}{h}\cos\overline{\lambda} - \sqrt{\frac{a_2b_1}{a_1b_2}}\cos\hat{\lambda}\frac{d}{h}\sin\overline{\lambda}} \cdot \frac{1}{(\omega-1)\sqrt{2\pi}}, \tag{33}$$

and

$$i\omega\overline{u}_1 = \frac{\sin\hat{\lambda}\left(x_1+\frac{d}{h}\right)}{\sin\hat{\lambda}\frac{d}{h}\cos\overline{\lambda} - \sqrt{\frac{a_2b_1}{a_1b_2}}\cos\hat{\lambda}\frac{d}{h}\sin\overline{\lambda}} \cdot \frac{1}{(\omega-1)i\sqrt{2\pi}}. \tag{34}$$

IV. Discussion

A. Bubble Size Distribution

Before calculating the steady-state response arising from the pole at $\omega = 1$, two simple cases of equilibrium bubble size distributions are noted. For a uniform distribution of equilibrium bubble radii $\overline{R}_0$, we have,

$$f(R_0, x_1) = N\delta(R_0 - \overline{R}_0), \tag{35}$$

where N is the number of bubbles per unit volume. Correspondingly, we find that

$$a_2 = \frac{3\beta_0}{1-\beta_0}\frac{p_0\omega_0 h}{\rho_0\nu_0} \cdot \frac{1}{[3\beta_0 c_0^2 - \omega^2\omega_0^2 R_0^2 - i\omega(2\pi)^{1/2}J_B(0)\overline{J}_{B1}/\rho_0]}, \tag{36}$$

where $\beta_0 = 4\pi\overline{R}_0^3 N/3$. For a discrete distribution of equilibrium radii $\overline{R}_{0j}, j = 1, 2, \cdots$,

$$f(R_0, x_1) = \sum_j N_j\delta(R_0 - \overline{R}_{0j}) \tag{37}$$

and

$$a_2 = \frac{4\pi}{1-\beta_0}\frac{p_0\omega_0 h}{\rho_0\nu_0} \cdot \sum_j \frac{N_j\overline{R}_{0j}^3}{[3\beta_0 c_{0j}^2 - \omega^2\omega_0^2\overline{R}_{0j}^2 - i\omega(2\pi)^{1/2}J_{Bj}(0)\overline{J}_{B1j}/\rho_0]}, \tag{38}$$

where c_{0j} is given by (26) with R_0 replaced by $\overline{R}_{0j}$ and β_0 is a sum over j. There may be a dependence of J_B on R_0, hence we have placed a subscript j on $J_{Bj}(0)$ and $\overline{J}_{B1j}$. More complicated distributions can also be handled with (25) once the appropriate distribution function is specified.

B. Relaxation in the Tissue

Dinnar [2] gives the following expression.

$$J_{T1}(t_1) = \left(\frac{J_T(\infty)}{J_T(0)} + \frac{t_1}{J_T(0)\omega_0 Q_1} + e^{-(\lambda/\omega_0)t_1}\left[1 - \frac{J_T(\infty)}{J_T(0)}\right]\right)H(t_1), \tag{39}$$

where $\lambda = Q_1/Q_2$ and $J_T(0) = P_2/Q_2$, and $J_T(\infty) = (P_1Q_1 - Q_2)/Q_1^2$. The Q_i and P_i are obtained from measurements. Typical values of Q_i and P_i for tissue are [2], [7] $Q_1 = 10^4 Ns/m^2, Q_2 = 1.8\times10^2 Ns^2/m^2, P_1 = 6.8\times10^{-2}s$ and $P_2 = 0.72 \times 10^{-3}s^2$. However, the linear dependence upon t_1 means that the Fourier transform of J_{T1} does not converge, except as a generalized function [6]. However, as indicated following (6), (39) is accurate only for small times. While we do not know the entire time history of the material, we can modify (39) in a way that preserves its behavior at small times. Accordingly, we write J_{T1} as

$$J_{T1}(t_1) = \left(\frac{J_T(\infty)}{J_T(0)} + e^{-(\lambda/\omega_0)t_1} \cdot \left[1 - \frac{J_T(\infty)}{J_T(0)} + \frac{t_1}{J_T(0)\omega_0 Q_1}\right]\right)H(t_1). \tag{40}$$

Note that λ/ω_0 is very small for the frequencies of interest. The transformed creep compliance is given by

$$\overline{J}_{T1}(\omega) = \frac{J_T(\infty)}{J_T(0)}\left[\frac{1}{\sqrt{2\pi}i\omega}\right] + \left(1 - \frac{J_T(\infty)}{J_T(0)}\right)\frac{1}{\sqrt{2\pi}}\frac{1}{i\omega + \lambda/\omega_0} - \frac{1}{\sqrt{2\pi}\omega_0 Q_1 J_T(0)}\frac{1}{(\omega - i\lambda/\omega_0)^2}. \tag{41}$$

Sometimes the transform of the Heaviside function is written with a $\delta(\omega)$ [6]. This can be ignored by noting that an inversion contour would pass below the pole at $\omega = 0$ because $\overline{J}_{T1}$ must be analytic in $\mathrm{Im}(\omega) < 0$ plane.

C. Relaxation in the Bubbly Liquid

An approximate expression for $\overline{J}_{B1}$ can be obtained by comparing with results given in Commander and Prosperetti [1]. That comparison gives,

$$\overline{J}_{B1} = -2\frac{\omega_0}{(2\pi)^{1/2}J_B(0)}\left[2\mu + \frac{p_{g0}}{2\omega\omega_0}\mathrm{Im}\,\Phi\right] + \frac{p_{g0}}{i\omega(2\pi)^{1/2}J_B(0)}(3 - \mathrm{Re}\,\Phi), \tag{42}$$

where μ is the viscosity of the fluid. The two real terms represent attenuation due to viscosity and heat transfer. Furthermore, we have

$$\Phi = \frac{3\gamma}{1 - 2(\gamma-1)i\chi[(i/\chi)^{1/2}\coth(i/\chi)^{1/2} - 1]}, \tag{43}$$

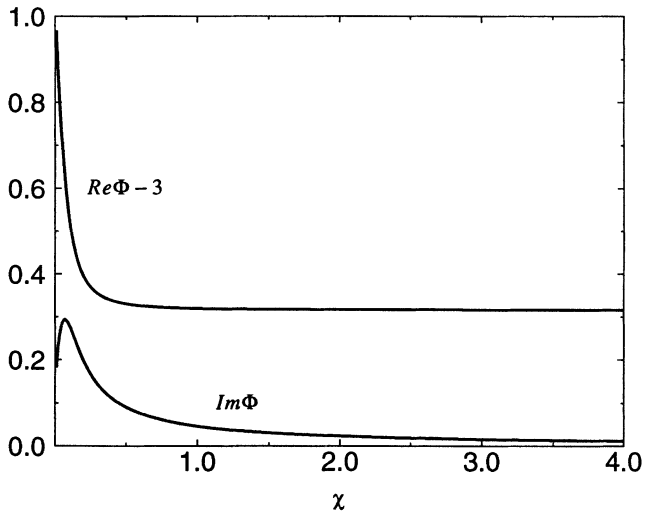

Fig. 2. Plots of (Re $\Phi-$ 3) and Im Φ for $\gamma = 1.4$ as a function of χ.

where γ is the ratio of the specific heats in the bubble, $\chi = D_g/(\omega\omega_0\overline{R}_0^2)$, and D_g is the gas thermal diffusivity. Note that the second term in (33) of [1] should be divided by the angular frequency. Equation (42) has been approximated for ω real and positive. To recover J_{B1} it must be continued as indicated below (12). For $\gamma = 1.4$ we plot both (Re $\Phi-$ 3) and Im Φ as a function of χ in Fig. 2.

The function J_{B1} can also be estimated in other ways. For example, Wijngaarden [11] indicates that the attenuation of a bubble oscillation with an equilibrium radius $\overline{R}_0$ of the order of 0.5–5 μm is primarily thermal. Moreover, it is suggested [11] that the following simple expression can be used for this range of bubble radii.

$$\begin{aligned}\mathrm{Re}(\overline{J}_{B1}) &= -\frac{\rho_0\overline{R}_0^2\omega\omega_0\omega_b}{(2\pi)^{1/2}J_B(0)}\delta_{th} \\ &= -4.45\times10^{-4}\frac{\rho_0\overline{R}_0^2(\omega\omega_0)^{1/2}\omega_b^2}{2\pi J_B(0)}, \qquad (44)\end{aligned}$$

where the term ω_b is the natural frequency for the oscillation of a single bubble and will be defined in (53). In comparing our work with that of [11] we have approximated $(1-\beta_0)$ as 1. Note that the inversion contour would pass below the branch point at $\omega = 0$. Examining Fig. 2, the term associated with (Re $\Phi-$ 3) has a less significant influence upon Ω^2 in (16) than the term associated with Im Φ has upon attenuation. Therefore, we approximate Im $(\overline{J}_{B1})$ as zero. Numerical estimates of Re $(\overline{J}_{B1})$ using either (42) or (44) show that they are of the same order of magnitude for the parameter values used here. Therefore, we shall use the simpler (44) for our numerical examples. Note that $\overline{J}_{B1j}$ is gotten by replacing $\overline{R}_0$ with $\overline{R}_{0j}$.

Using (44), the attenuation coefficient per unit length D in the bubbly liquid in the free field is

$$D = 8.69\left[\frac{2\times4.45\times10^{-4}}{3(2\pi)^{1/2}}\frac{\omega_0^{3/2}}{c^3}(\overline{R}_0\omega_b)^2\right]\mathrm{dB/m} \qquad (45)$$

where c is the sound speed in the liquid without bubbles. For $f_0 = \omega_0/2\pi = 30$ kHz, we find $D = (0.02, 0.68, 0.74)$ dB/cm for $\overline{R}_0 = (0.5, 5, 50)$ μm.

O'Brien and Smith [8] estimated the attenuation in bubbly water at 30 kHz under typical HYDROSOUND^{TM} system operating conditions, in which tap water is delivered to a tub through a tapered jetway (Arjo, Inc., Morton Grove, IL). The tub in which the measurements were conducted was lined with rubber mats to add a degree of ultrasonic attenuation along the tub surface to simulate more closely free-field exposure conditions. Three complete measurement scans were initiated within 20 to 30 minutes from the time the tub was filled with water and were conducted in series. Each scan required about 15 minutes.

The measurements were made using a calibrated NRL (Transducer Branch of the U.S. Naval Research Laboratory's Underwater Sound Reference Detachment, Orlando, FL) Type F42D hydrophone (sensitivity 37.6 kPa/V at 30 kHz). The measurement scanning geometry consisted of seven planes parallel to and located along the beam axis at ranges of 2 cm, 22 cm, 42 cm, 62 cm, 82 cm, 102 cm and 122 cm from the transducer face. Each plane consisted of 1600 data points (a 40 × 40 grid) which were sampled every 0.5 cm, that is, the dimension of each plane was 20 cm × 20 cm. The HYDROSOUND^{TM} transducer has an active rectangular source area 16 cm horizontally × 11 cm vertically (a 32 × 22 grid).

The attenuation coefficients between adjacent planes for each of the tests were determined by calculating the decrease (in dB) in each plane's maximum pressure amplitude between two adjacent planes (20 cm separation) and the individual attenuation coefficient values were averaged to yield a mean (standard deviation) attenuation coefficient of 0.43 (0.12) dB/cm. This compares favorably with the estimates given below (45). One might infer from the comparison that the equilibrium radii probably fall within the range of 0.5 to 5 μm.

D. Steady-State Solutions

Recalling the expressions for $\hat{\lambda}, \overline{\lambda}, a_1, a_2, b_1$ and b_2, we see that possible branch points and poles come from $a_2 \to \infty$ and $b_2 = 0$, or, using (38),

$$3\beta_0 c_{0j}^2 - \omega^2\omega_0^2\overline{R}_{0j}^2 - i\omega(2\pi)^{1/2}J_{Bj}(0)\overline{J}_{B1j}(\omega)/\rho_0 = 0 \quad (46)$$

and

$$i\omega\overline{J}_{T1}(\omega) = 0. \qquad (47)$$

These points and any poles that arise from the common factor in the denominator of (31)–(34) are in the Im(ω) >0 half plane, correspond to the transient solutions and will be damped out leaving the steady-state response from the pole at $\omega = 1$. Resonances will occur when the branch points or poles lie near $\omega = 1$. Most poles indicate resonances caused by the layering. Note that the positions of the poles and branch points depend on ω_0 because of our normalization.

The steady-state solutions are

$$p_1=-\left\{\sqrt{\frac{a_1}{a_2}}\frac{\sin\hat{\lambda}\frac{d}{h}\sin\overline{\lambda}x_1+\sqrt{\frac{a_2b_1}{a_1b_2}}\cos\hat{\lambda}\frac{d}{h}\cos\overline{\lambda}x_1}{\sin\hat{\lambda}\frac{d}{h}\cos\overline{\lambda}-\sqrt{\frac{a_2b_1}{a_1b_2}}\cos\hat{\lambda}\frac{d}{h}\sin\overline{\lambda}}\right\}\Bigg|_{\omega=1} ie^{it_1} \tag{48}$$

$$\nu_1=\left\{\frac{\sin\hat{\lambda}\frac{d}{h}\cos\overline{\lambda}x_1-\sqrt{\frac{a_2b_1}{a_1b_2}}\cos\hat{\lambda}\frac{d}{h}\sin\overline{\lambda}x_1}{\sin\hat{\lambda}\frac{d}{h}\cos\overline{\lambda}-\sqrt{\frac{a_2b_1}{a_1b_2}}\cos\hat{\lambda}\frac{d}{h}\sin\overline{\lambda}}\right\}\Bigg|_{\omega=1} e^{it_1}, \tag{49}$$

$$\sigma_1=\left\{\sqrt{\frac{b_1}{b_2}}\frac{\cos\hat{\lambda}\left(x_1+\frac{d}{h}\right)}{\sin\hat{\lambda}\frac{d}{h}\cos\overline{\lambda}-\sqrt{\frac{a_2b_1}{a_1b_2}}\cos\hat{\lambda}\frac{d}{h}\sin\overline{\lambda}}\right\}\Bigg|_{\omega=1} ie^{it_1}, \tag{50}$$

and

$$iu_1=\left\{\frac{\sin\hat{\lambda}\left(x_1+\frac{d}{h}\right)}{\sin\hat{\lambda}\frac{d}{h}\cos\overline{\lambda}-\sqrt{\frac{a_2b_1}{a_1b_2}}\cos\hat{\lambda}\frac{d}{h}\sin\overline{\lambda}}\right\}\Bigg|_{\omega=1} e^{it_1}, \tag{51}$$

where $t_1 \geq 0$.

E. Bubble Resonance: $a_2 \to \infty$

From (38) the bubble resonances occur for

$$c_{0j}^2-\frac{\omega^2\omega_0^2}{3\beta_0}\overline{R}_{0j}^2-i\omega\frac{\sqrt{2\pi}J_{Bj}(0)\overline{J}_{B1j}(\omega)}{3\beta_0\rho_0}=0, \qquad j=1,2,\cdots \tag{52}$$

where subscript j is kept to denote a possible discrete distribution of equilibrium bubble sizes. Therefore, when $\overline{J}_{B1j}=0$ this limit is equivalent to

$$\omega^2\omega_0^2\to\left(\frac{3p_{g0}}{\rho_0}-\frac{2\Gamma}{\rho_0\overline{R}_{0j}}\right)\frac{1}{\overline{R}_{0j}^2}=\omega_0^2\Omega_j^2\equiv\omega_{bj}^2, \qquad j=1,2,\cdots \tag{53}$$

From [9], ω_{bj} is the natural frequency for the oscillation of a single bubble with equilibrium radius $\overline{R}_{0j}$. Consequently, for this case $\omega=1$ corresponds to driving the bubbly liquid at one of the bubble resonant frequencies.

Note that the right hand sides of (48)–(51) at $\omega=1$ are indeterminate in this case. These indeterminate solutions may be explained as a consequence of an increase in the scattering cross section [1] in the neighborhood of the bubble resonant frequency. Most of the input energy is being scattered by resonant bubbles at the surface of the transducer and little is left to penetrate the bubbly liquid and be delivered to the tissue surface.

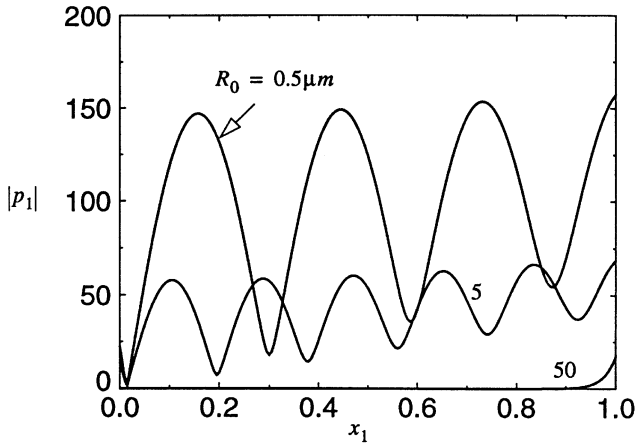

(a)

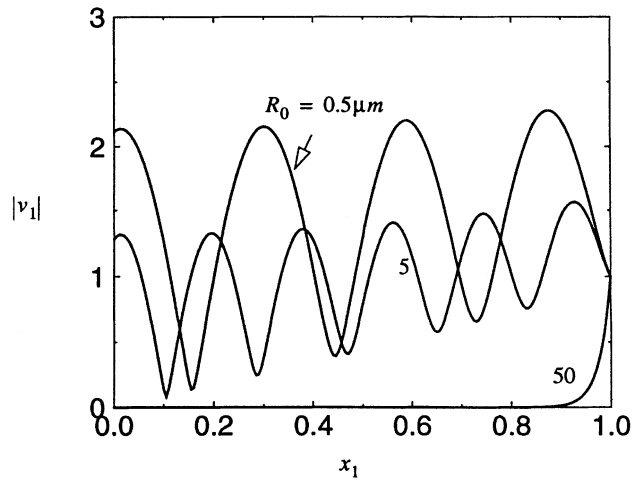

(b)

Fig. 3. The magnitude of (a) the acoustic pressure $|p_1|$ and (b) the particle velocity $|\nu_1|$ are plotted against x_1 for $\overline{R}_0$ equals 0.5 μm, 5 μm and 50 μm, respectively. The frequency f_0 = 30 kHz.

F. Numerical Examples

Using the values for the P_i and the Q_i given below (39), we obtain $J_T(0)=4\times10^{-6}\,\mathrm{m}^2/\mathrm{N}$, $J_T(\infty)=5\times10^{-6}\,\mathrm{m}^2/\mathrm{N}$ and $\lambda=5.56\times10\ \mathrm{s}^{-1}$. From these we find that

$$\sqrt{2\pi}i\overline{J}_{T1}(1)\approx1-2.07\times10^{-4}i. \tag{54}$$

The intensity of the acoustic wavefield is taken to be $I=1200\ \mathrm{W/m}^2$ (typical for the HYDROSOUND^{TM} system) so that $\nu_0=4$ m/s and $\epsilon=0.01$. Furthermore, we assume that $d=1$ mm, $h=10$ cm, $\rho_s=1100\ \mathrm{kg/m}^3$, $\rho_0=1000\ \mathrm{kg/m}^3$, and $\beta_0=10^{-4}$. The ambient pressure is assumed to be atmospheric, that is, $p_0=10^5$Pa and the surface tension coefficient is taken to be $\Gamma=0.073$ Pa/m. We choose the driving frequency and the equilibrium bubble radius as variable parameters. However, we shall assume that there is only a single bubble radius for each case.

Fig. 3 gives the magnitudes of (a) the acoustic pressure $|p_1|$ and (b) the particle velocity $|\nu_1|$ in the bubbly liquid for a

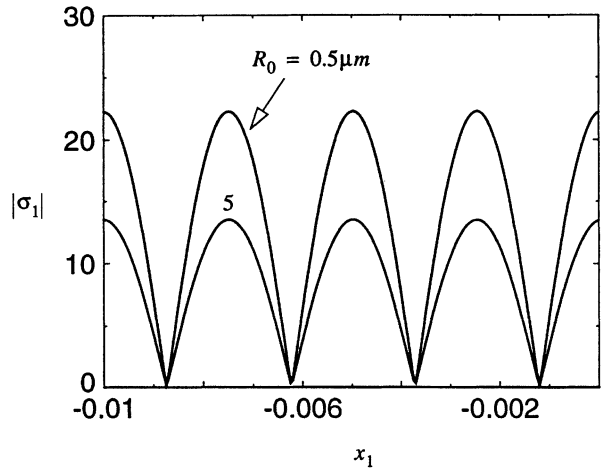

(a)

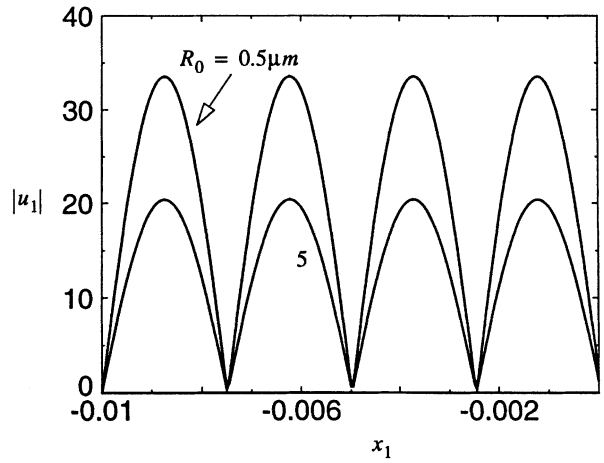

(b)

Fig. 4. The magnitude of (a) the normal component of traction $|\sigma_1|$ and (b) the particle displacement $|u_1|$ are plotted against x_1 for $\overline{R}_0$ equals 0.5 μm, 5 μm and 50 μm, respectively. The frequency $f_0 = 30$ kHz.

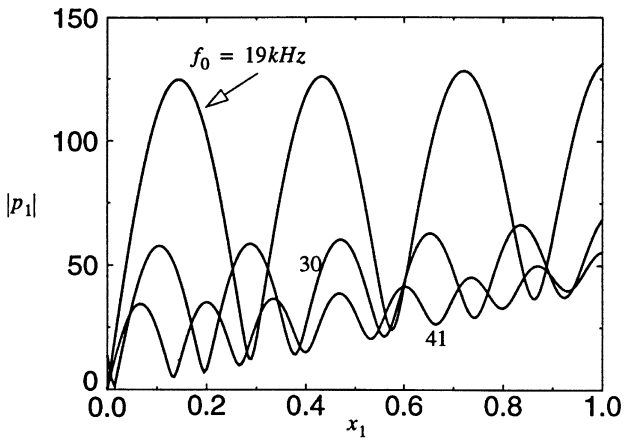

(a)

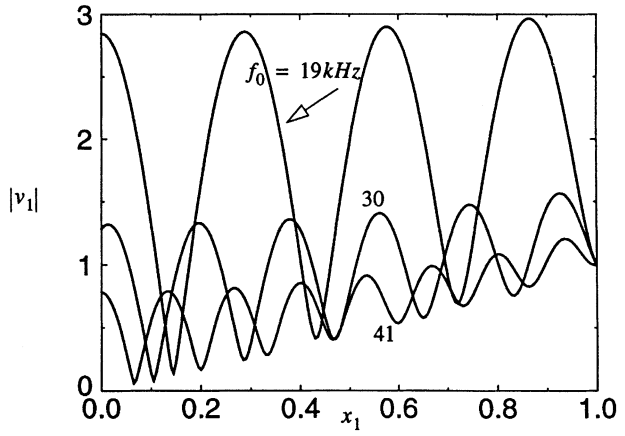

(b)

Fig. 5. The magnitude of (a) the acoustic pressure $|p_1|$ and (b) the particle velocity $|\nu_1|$ are plotted against x_1 for f_0 equals 19 kHz, 30 kHz and 41 kHz, respectively. The equilibrium bubble radii $\overline{R}_0 = 5$ μm.

driving frequency $f_0 = 30$ kHz and three different equilibrium bubble radii $\overline{R}_0 = 0.5$, 5 and 50 μm. The amplitude of the spatial oscillation decreases with the increase of equilibrium bubble radii and the spatial periodicity is also affected by the variation of $\overline{R}_0$. The pressure and velocity amplitudes associated with $R_0 = 50$ μm are negligible.

Fig. 4 gives the magnitude of (a) the normal component of traction $|\sigma_1|$ and (b) the displacement in the tissue $|u_1|$ for the same driving frequency $f_0 = 30$ kHz and equilibrium bubble radii $\overline{R} = 0.5$ and 5 μm. In contrast to case of the bubbly liquid, the spatial periodicity is not affected by the variation of $\overline{R}_0$. The amplitude of the spatial oscillation decreases with the increase of equilibrium bubble radii. There is no appreciable spatial attenuation in the tissue because of its low attenuation. This may indicate that the viscoelastic model may not accurately capture the frequency response of the tissue.

Fig. 5 gives the magnitudes of (a) the acoustic pressure $|p_1|$ and (b) the particle velocity $|\nu_1|$ in the bubbly liquid for an equilibrium bubble radii $\overline{R}_0 = 5$ μm and three different driving frequencies $f_0 = 19$, 30, and 41 kHz. Higher driving frequencies lead to more significant spatial attenuation.

A nonmonotonic amplitude variation of both the normal component of the traction $|\sigma_1|$ and the displacement $|u_1|$ in the tissue can be observed from Fig. 6. Here, $f_0 = 30$ kHz is seen to excite the largest response in the tissue and $f_0 = 41$ kHz leads to the smallest. This happens because the finite thicknesses of the bubbly liquid and tissue layers introduce a set of natural frequencies. In fact, the denominator in (47)–(50) can be shown to have a zero near $f_0 = 30$ kHz if the attenuation in both the bubbly liquid and the tissue layer are small.

Fig. 7 gives the magnitudes of (a) the acoustic pressure $|p_1|$ and (b) the particle displacement $|u_1|$ as a function of the driving frequency $f_0 = \omega_0/2\pi$ at the tissue surface for an equilibrium bubble radius $\overline{R}_0 = 5$ μm. Note that $\overline{J}_{B1}$ may not be accurate over the full range of frequencies used. The resonant behavior is quite sharp. Careful comparison of the results for Figs. 5, 6 and 7 show that $|p_1| = |\sigma_1| \approx 14$ for $f_0 = 30$ kHz at $x_1 = 0$. However, Fig. 7 shows that a slight increase in f_0 increases $|p_1|$ significantly.

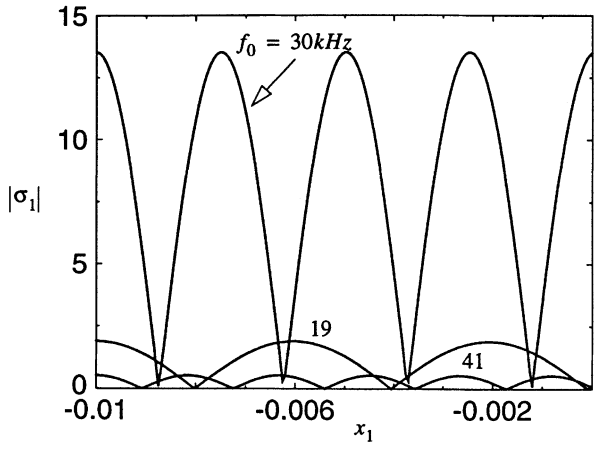

(a)

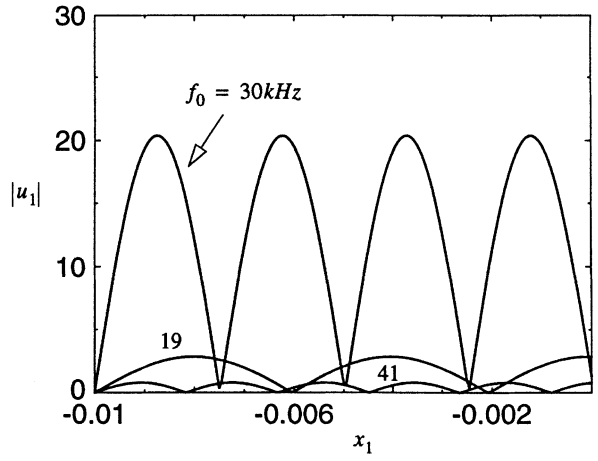

(b)

Fig. 6. The magnitude of (a) the normal component of traction $|\sigma_1|$ and (b) the particle displacement $|u_1|$ are plotted against x_1 for f_0 equals 19 kHz, 30 kHz and 41 kHz, respectively. The equilibrium bubble radii $\overline{R}_0 = 5\ \mu\mathrm{m}$.

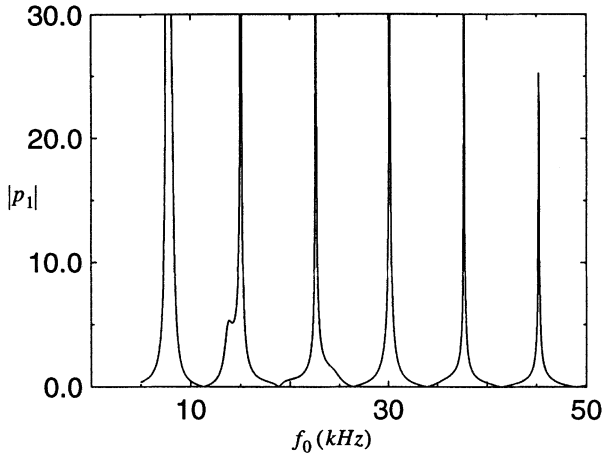

(a)

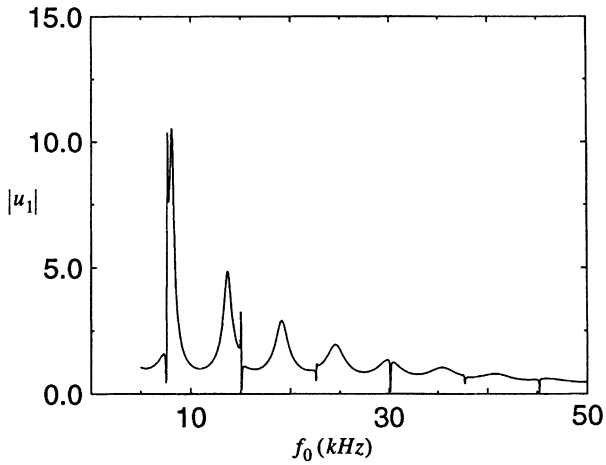

(b)

Fig. 7. The magnitude of (a) the acoustic pressure $|p_1|$ and (b) the particle displacement $|u_1|$ are plotted against the frequency f_0 at the tissue surface $x_1 = 0$. The equilibrium bubble radii $\overline{R}_0 = 5\ \mu\mathrm{m}$.

Finally, the resonant bubble frequencies are found to be $f_b = 9 \times 10^2$, 5.24×10^2, and 54.8 kHz for $\overline{R}_0 = 0.5$, 5 and 50 μm, respectively. Clearly all are above the driving frequencies used in the numerical calculations. Also, corresponding to a driving frequency of 30 kHz, the resonant bubble radius is found to be 92.2 μm.

V. Concluding Remarks

A linear model for propagation in a layered structure comprising a bubbly liquid adjacent to a viscoelastic solid, that models tissue, has been proposed and explored. It depends upon three functions $f(R_0, x_1), J_T(t_1)$ and $J_B(t_1)$ whose form can be estimated either from theory or measurement. It is clear that propagation will not take place efficiently unless the spectrum of resonant frequencies for the bubbles is avoided. The numerical results indicate the spatial distributions of pressure and velocity in the bubbly liquid, and traction and displacement in the tissue. Specifically, spatial attenuation is observed in the bubbly liquid and is more significant for higher driving frequencies. In contrast, little spatial attenuation is observed in the tissue using the present model. The layering introduces sharp resonances.

References

[1] K. W. Commander and A. Prosperetti, "Linear pressure waves in bubbly liquids: Comparison between theory and experiments," *J. Acoust. Soc. Am* ., vol. 85, pp. 732–746, 1989.
[2] U. Dinnar, "A note on the theory of deformation in compressed skin tissues," *Math. Biosci.*, vol. 8, pp. 71–82, 1970.
[3] D. C. Gibson and J. R. Blake, "The growth and collapse of bubbles near deformable surface," *Appl. Sci. Res*., vol. 38, pp. 215–224, 1982.
[4] I. Hanson, V. Kedrinskii, and K. A. Morch, "On the dynamic of cavity clusters," *J. Phys. D: Appl. Phys*., vol. 15, pp. 1725–1735, 1982.
[5] D. Y. Hsieh, "On dynamics of bubbly liquids," in *Advances in Applied Mechanics*, J. W. Hutchinson and T. Y. Wu, Eds. New York: Academic Press, 1988, vol. 26, pp. 63–133.
[6] M. J. Lighthill, *Fourier Analysis and Generalized Functions.* Cambridge: The University Press, 1970, pp. 42–44.
[7] W. L. Nyborg, *Intermediate Biophysical Mechanics.* Menlo Park, CA: Cummings, 1975, pp. 216–219.
[8] W. D. O'Brien Jr. and N. B. Smith, unpublished report to Arjo., Inc., Morton Grove, IL, 1994.
[9] M. S. Plesset and A. Prosperetti, "Bubble dynamics and cavitation," M. Van Dyke, J. V. Wehausen, and J. L. Lumley, Eds. *Annu. Rev. Fluid Mech*., vol. 9, pp. 145–185, 1977.
[10] V. Wijngaarden, "On the equations of motion for mixtures of liquid and gas bubbles," *J. Fluid Mech*., vol. 33, pp. 465–474, 1968.

[11] _____, "One-dimensional flow of liquids containing small gas bubbles," M. Van Dyke, W. G. Vincenti, and J. V. Wehausen, Eds. *Ann. Rev. Fluid Mech*., vol. 4, pp. 369–390, 1972.

Quan Qi attended Xi'an Jiaotong University and graduated with a B.S. degree in engineering mechanics in 1982. Then he went on to pursue graduate studies at the Research Institute of Petroleum Exploration in Beijing, China and he received his M.E. degree in petroleum exploration in 1984. After working as a research assistant at Xi'an Petroleum Institute for two years, he began his Ph.D. studies at the University of Illinois at Urbana-Champaign. In May 1990 he was awarded a M.S. degree and in October 1992 he obtained his Ph.D. degree in both theoretical and applied mechanics.

Presently he is with the Department of Theoretical and Applied Mechanics at University of Illinois. His research interests include nonlinear acoustic and ultrasonic applications, fluid mechanics and materials processing, and dynamics and vibration analysis.

Dr. Qi is a member of the Acoustical Society of America and American Society of Mechanical Engineers. He was the recipient of 1992-1993 Hunt Postdoctorate Fellowship of the Acoustical Society of America.

John G. Harris received the B.Eng. Hon. in electrical engineering in 1971 from McGill University, Montreal, PQ and the Ph.D. in applied mathematics in 1979 from Northwestern University, Evanston, IL.

He then joined the Department of Theoretical and Applied Mechanics at the University of Illinois in Urbana where he is now a Professor. He is responsible for teaching dynamics and physical acoustics in both fluids and solids. His research interests are mainly in asymptotic descriptions of linear wave propagation and diffraction, but he also has an increasing interest in nonlinear waves.

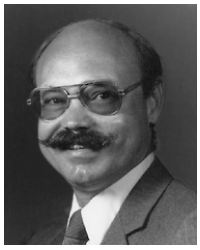

William D. O'Brien Jr. (S'64–M'70–SM'79–F'89) received the B.S., M.S., and Ph.D. degrees in 1966, 1968, and 1970, from the University of Illinois, Urbana-Champaign.

From 1971 to 1975 he worked with the Bureau of Radiological Health (currently the Center for Devices and Radiological Health) of the U.S. Food and Drug Administration. Since 1975, has been at the University of Illinois, where he is a Professor of Electrical and Computer Engineering and of Bioengineering, College of Engineering, and Professor of Bioengineering, College of Medicine, and is the Program Director of the Radiation Biophysics and Bioengineering in Oncology Training Program. His research interests involve the many areas of ultrasound-tissue interaction, including spectroscopy, risk assessment, biological effects, tissue characterization, dosimetry, blood-flow measurements, acoustic microscopy and meat characterization for which he has published more than 150 papers.

Dr. O'Brien is Editor-in-Chief of the IEEE TRANSACTIONS ON ULTRASONICS, FERROELECTRICS, AND FREQUENCY CONTROL. He is a Fellow of IEEE, the Acoustical Society of America, and the American Institute of Ultrasound in Medicine (AIUM) and was recipient of an IEEE Centennial Medal (1984), the AIUM Presidential Recognition Awards (1985 and 1992), the AIUM/WFUMB Pioneer Award (1988), the IEEE Outstanding Student Branch Counselor Award (1989), and the AIUM Joseph H. Holmes Basic Science Pioneer Award (1993). He was recently inaugurated as a Founding Fellow of American Institute of Medical and Biological Engineering. He was President (1982-1983) of the IEEE Sonics and Ultrasonics Group (currently the IEEE UFFC-Society), Co-Chairman of the 1981 IEEE Ultrasonic Symposium, and General Chairman of the 1988 IEEE Ultrasonics Symposium. He was also President of the AIUM (1988–1991) and Treasurer of the World Federation for Ultrasound in Medicine and Biology (1991–1994).